ELSEVIER

Cement & Concrete Composites 25 (2003) 253–261

Cement & Concrete Composites

www.elsevier.com/locate/cemconcomp

Strength and fracture resistance of FRP reinforced concrete flexural members

Z.J. Wu [a], J.Q. Ye [b,*]

[a] Manchester School of Engineering, The University of Manchester, Manchester M13 9PL, UK
[b] Department of Civil Engineering, School of Civil Engineering, University of Leeds, Leeds LS2 9JT, UK

Received 17 May 2001; accepted 8 March 2002

Abstract

A theoretical method to predict the loading capacity and fracture resistance of FRP reinforced concrete flexural beams is developed. No slip between FRP rods and plain concrete matrix is assumed and only Mode I fracture propagation is considered. The model is valid for any crack length and for any span-to-depth ratio larger than 2.5. The influence of the bridging stresses provided by the fracture process zone at the tip of fictitious fracture is examined. The numerical results are compared with existing experimental results which were obtained for steel reinforcement.

Keywords: Mode I fracture; FRP rod; Concrete beam; Fracture resistance

1. Introduction

Plain concrete has traditionally been regarded as quasi-brittle because it exhibits a moderately tension-weak behaviour and its tensile strength is only about one-tenth of its compressive strength [1]. Hence, plain concrete structures normally fail due to propagation of tensile cracks. In engineering applications, the tension resistance of concrete is usually increased by using different types of reinforcement. In recent years, fiber reinforced plastic (FRP) rods or bars, which offer corrosion resistance and provide nonconductive/magnetic properties, have been increasingly used in civil engineering. This has been shown by the latest ACI state-of-the-art report on FRP reinforcement for concrete structures [2]. FRP reinforced concrete structures are now considered as a potential replacement for traditional steel reinforcing concrete in many engineering applications such as smart structures, structures under corrosive environments and structural elements required to have a high strength/weight ratio.

The use of FRP reinforcements for concrete structures depends on their ability to perform reliably under service loads [3]. The mechanical properties, e.g., strength and toughness properties, of the reinforcements are the most important properties if the reinforced structures are used as load-bearing members. Although there are some published results [2,4] about structural designs of FRP reinforcement products, most of them are developed on the basis of the classical strength and stiffness criteria which cannot be used satisfactorily to predict or estimate service reliability of the FRP structural members, particularly, when cracks are present. It is known that for reinforced concrete structures the presence of FRP reinforcements may have little effect on the initiation of a crack, but they do provide considerable resistance to both propagation and opening of the crack. Cracks generally initiate at the locations where the principal tensile stress (or the strain energy release rate) exceeds the material tensile strength (or the fracture toughness) under service loads. Further propagation of these cracks will depend on the distributions and magnitudes of both principal tensile stress and material fracture resistance. In general, the mechanical performance, failure modes, and loading capacity of a reinforced concrete structure depend on, not only its structural geometry and loading conditions, but also the amount, location, and

* Correspondence author. Fax: +44-0113-2332265.
E-mail address: j.ye@leeds.ac.uk (J.Q. Ye).

0958-9465/03/$ - see front matter
PII: S0958-9465(02)00015-X

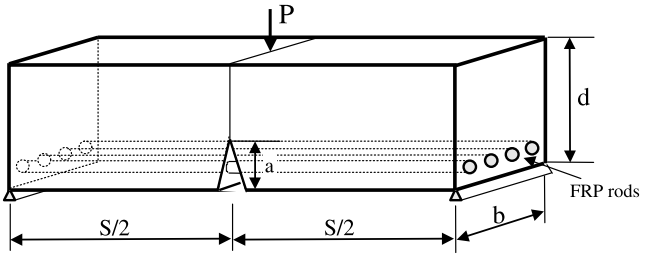

Fig. 1. Three-point bending of a FRP reinforced concrete beam with a rectangular cross-section.

orientation of the FRP reinforcement used [5]. More research in this area is needed.

In the present research, a flexural FRP reinforced concrete beam with a rectangular cross-section and subjected to an external loading system of three-point bending is considered. Along the axial direction, the beam is reinforced with unidirectional FRP rods near the bottom surface of the tensile zone (Fig. 1). It is our objective to develop a theoretical method to predict the loading capacity and fracture resistance of such a FRP reinforced concrete structure. The research is based on the consideration of the constitutive relationships and deformation properties of the individual constituents, i.e., plain concrete and FRP rods. From the global equilibrium of the cracked cross-section, the change of the load-bearing capacity of the beam against crack depth is determined. A fictitious crack approach which has been used previously in conjunction with the finite element method [6,7] in the fracture analysis of concrete is adopted here to estimate the equivalent bridging effect of the fracture process zone (FPZ) of the concrete. The focus of the paper is on the analytical solution of crack growth resistance, including the toughening effect of FRP rods. The paper is structured as follows: Section 2 gives the constitutive relationships of plain concrete and FRP rods which will be used as the basis of the model to be developed. Load-bearing capacity of the FRP reinforced concrete beam and the corresponding crack growth resistance curves are, respectively, presented in Sections 3 and 4. The numerical results in Section 5 demonstrate that the loading capacity obtained from present model agree with the results from experimental tests. The effect of the FPZ on fracture toughness and resistance is then shown graphically. Conclusions are given in Section 6.

2. Constitutive relationships of plain concrete and FRP rod

The behaviour of tension-weak plain concrete is basically characterized by a linear stress–strain relationship up to the ultimate tensile strength although there is

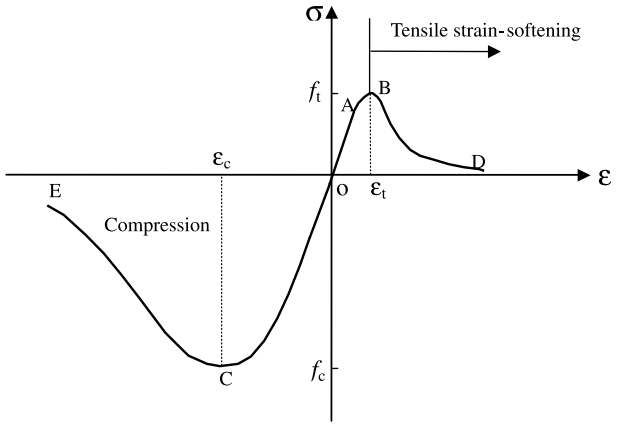

Fig. 2. Stress–strain curves for plain concrete.

a slight strain hardening due to diffuse progressive damage of the material under increasing tensile stress. Beyond the ultimate tensile strength or maximum stress, further strain increase gives a decreasing stress, which is commonly called 'strain-softening' behaviour [8] (Fig. 2). Strictly speaking, after the maximum load or stress, the definition of strain is lost because a discrete crack now opens up and widens with increasing strain, whilst still being bridged by tortuous segments caused mainly by the opening of FPZ [9] (Fig. 3). Many studies have shown that the softening (descending) part of the tensile stress–strain curve shown in Fig. 2 is not purely a material property [5], since the response depends on the dimensions of the specimen, the loading rate and the gage length used for measurement. It is assumed that such strain localization appears only after the maximum load is reached. As a result of the strain localization, softening behaviour of plain concrete should be described by using a stress (q)–displacement (w) relationship, which may be considered as a material property [10], rather than the stress–stain relationship shown in Fig. 2. There are a number of strain-softening models that can be used in the analysis of FPR reinforced concrete. These models are all presented in the form of stress versus displacement, i.e., $q(w)$, which include lin-

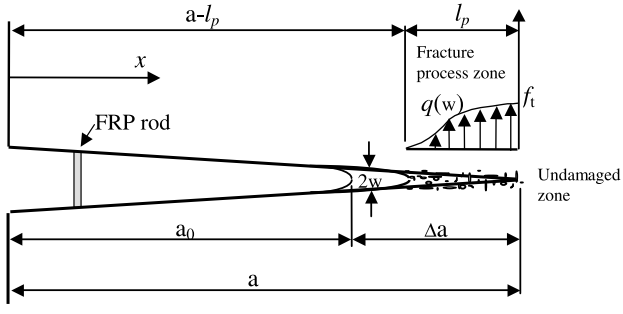

Fig. 3. Sketch of FRP reinforced concrete crack and FPZ.

ear (used in Hillberborg's original fictitious crack model [6]), bilinear [11], trilinear [12], exponential [13] and power [6,14] functions. It has been demonstrated that the choice of $q(w)$ influences the prediction of structural responses significantly [15]. Hence, the selection of $q(w)$ becomes very important. In this paper, the constitutive law of the stress–displacement relationship for describing the tensile softening of plain concrete is not specified, i.e., an arbitrary $q(w)$ is adopted in the theoretical analysis. Numerical calculations are reported for two extreme cases, i.e., the upper and lower limit analyses, to show the influence of the choice of $q(w)$.

To account for concrete behaviour in the compressive zone of the beam, the empirical parabolic curve proposed by Hognestad [5] to describe the compressive stress–strain relationship is adopted, as follows:

$$\sigma = f_c\left[2\frac{\varepsilon}{\varepsilon_c} - \left(\frac{\varepsilon}{\varepsilon_c}\right)^2\right], \tag{1}$$

where f_c and ε_c are the maximum compressive stress and the corresponding strain of concrete, respectively. Hence, along with the relationships between stress and strain/displacement in the tensile zone, the complete constitutive response of the plain concrete can be represented mathematically as follows:

$$\sigma = \begin{cases} q(w) & (\varepsilon \geqslant \varepsilon_t, \text{tensile softening}), \\ E\varepsilon & (0 \leqslant \varepsilon \leqslant \varepsilon_t, \text{tensile}), \\ f_c\left[2\dfrac{\varepsilon}{\varepsilon_c} - \left(\dfrac{\varepsilon}{\varepsilon_c}\right)^2\right] & (0 \leqslant |\varepsilon| \leqslant 2\varepsilon_c, \text{compessive}). \end{cases} \tag{2}$$

It should be noted that the peak stress f_t shown in Fig. 2 is different from the conventional concrete tensile strength obtained from a simple tensile test [5]. The latter depends on the material as well as the size and geometry of the test specimen and the test procedure, whereas the former, a size-independent value of tensile strength, is regarded as a material fracture parameter. According to Shah et al. [5], it can be measured consistently and easily by experiments.

The FRP rods in reinforced concrete structures are normally used to carry tensile stresses. The stress–strain laws of the FRP rods (glass fiber or carbon FRP rods) used in civil engineering are almost linearly elastic up to their ultimate strength. The tensile loads carried by the FRP rods are transferred to the concrete through the bond at the interface of the FRP rods and concrete. To facilitate the investigation of the fracture behaviour of the reinforced beam, a perfect bond between the FRP rods and the concrete is assumed (no slip effect is considered).

3. Load-bearing capacity of the FRP reinforced concrete beam

Consider the FRP reinforced concrete beam shown in Fig. 1. The beam has a rectangular cross-section and a notch or precrack a_0 at the mid-span. Assume that a_0 is larger than $(d - d_1)$, where $(d - d_1)$ is the distance from the FRP rods to the bottom surface of the beam (Fig. 4a). When the beam is loaded, the crack propagates to a, in which a FPZ (Fig. 3) is included. According to Hillberborg's fictitious crack model [6], the bridging stress in the FPZ is normal to the crack surface and can be given by the softening stress-separation law of plain concrete. Assuming that a plane section remains plane after deformation, a linear distribution of strain over the beam depth is obtained (Fig. 4b). Combining this strain distribution and the constitutive relationships for both concrete and FRP rods, the stress distributions on the cross-section at the mid-span of the beam are shown in Fig. 4c.

The modulus of concrete can be obtained from Fig. 2 and Eq. (2), i.e.,

$$E = \left.\frac{\partial\sigma}{\partial\varepsilon}\right|_{\varepsilon=0}. \tag{3}$$

Substituting (2) into (3) gives

$$E = \frac{2f_c}{\varepsilon_c}. \tag{4}$$

The resultant force in the compression zone of the concrete is given by

$$S = \int_{x_1}^{d} \sigma b\,\mathrm{d}x = \int_{x_1}^{d} bf_c\left[\frac{2\varepsilon}{\varepsilon_c} - \left(\frac{\varepsilon}{\varepsilon_c}\right)^2\right]\mathrm{d}x, \tag{5}$$

where

$$\varepsilon = \frac{x - x_1}{x_1 - a}\varepsilon_t \quad (d \geqslant x \geqslant x_1), \tag{6}$$

x_1 is the depth of the neutral axis from the bottom of the beam where the origin of x lies. ε_t is the tensile cracking strain in the concrete and is computed as

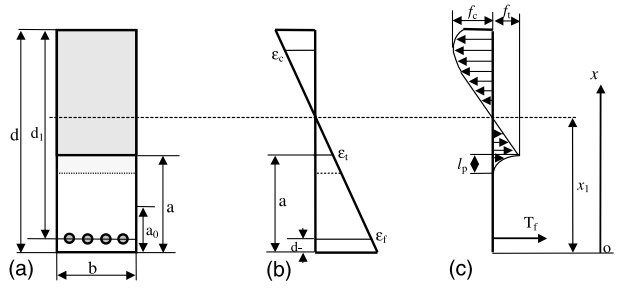

Fig. 4. Distributions of strain and stress across beam section at symmetrically cracked plane: (a) crack configuration, (b) strain distribution and (c) stress distribution.

$$\varepsilon_t = f_t/E. \tag{7}$$

The resultant tensile force on the cross-section consists of contributions from three parts: the tensile stress in concrete following the linear elastic law given by $\sigma = E\varepsilon$ from zero to f_t, the assumed stress distribution in the vicinity of the crack tip, i.e., the FPZ, and the tensile force due to the extension of the FRP rods. From Fig. 4c, the resultant, T, can be expressed by

$$T = \frac{1}{2} f_t (x_1 - a) b + \int_{a-l_p}^{a} q(w) b \, dx + T_f \tag{8}$$

in which l_p is the length of the FPZ, $q(w)$ is the distribution function of bridging closure stress in the zone, and $w = w(x)$ is one half of crack opening displacement (Fig. 3). T_f, shown in Fig. 4c, is expressed by

$$T_f = A_f E_f \varepsilon_f, \tag{9}$$

where E_f and A_f are, respectively, the longitudinal modulus and total area of the reinforced FRP rods. The corresponding strain ε_f is given by

$$\varepsilon_f = \frac{x_1 - (d - d_1)}{x_1 - a} \varepsilon_t. \tag{10}$$

The equilibrium of the beam requires that (5) must be equal to (8), i.e.,

$$A_f E_f \frac{x_1 - d_0}{x_1 - a} \varepsilon_t + \frac{1}{2} f_t (x_1 - a) b + F_p = b f_c \frac{(d - x_1)^2}{x_1 - a} \left[\frac{\varepsilon_t}{\varepsilon_c} - \frac{\varepsilon_t^2}{3\varepsilon_c^2} \frac{d - x_1}{x_1 - a} \right] \tag{11}$$

in which $d_0 = d - d_1$ and $F_p = \int_{a-l_p}^{a} q(w) b dx$ is the resultant bridging force provided by the FPZ which satisfies

$$0 \leqslant F_p < b l_p f_t. \tag{12}$$

Obviously, the lower and the upper limits of F_p are corresponding to the cases of zero length l_p and uniform distribution f_t along the process zone, respectively.

From Eqs. (4) and (7), it is seen that

$$\frac{\varepsilon_t}{\varepsilon_c} = \frac{1}{2} \frac{f_t}{f_c}. \tag{13}$$

Substituting (13) into Eq. (11) and letting $\alpha = a/d$, $\overline{y} = x_1/d - \alpha$, the equilibrium Eq. (11) becomes

$$\overline{y}^3 - 3\left[(1-\alpha)\left(1 + \frac{4f_c}{f_t}\right) + \frac{4f_c}{f_t}\left(\frac{F_p}{bdf_t} + \frac{A_f n}{bd}\right)\right]\overline{y}^2 + 3\left[(1-\alpha)^2\left(1 + \frac{2f_c}{f_t}\right) - \frac{4f_c}{f_t}\frac{A_f n}{bd}\left(\alpha - \frac{d_0}{d}\right)\right]\overline{y} - (1-\alpha)^3 = 0, \tag{14}$$

from which $\overline{y}$ and hence the location of the neutral axis can be determined if F_p is known. $n = E_f/E$ in Eq. (14) is the modulus' ratio of the FRP rods and plain concrete.

Following a similar procedure as used to derive (14), the bending moment due to the internal stresses on the symmetric cracked cross-section is given by

$$M = bd^2 f_t \left[\frac{A_f n}{bd} \frac{1}{\overline{y}} \left(\overline{y} + \alpha - \frac{d_0}{d} \right)^2 + \frac{\overline{y}^2}{3} + \frac{(1 - \alpha - \overline{y})^3}{\overline{y}} \left(\frac{1}{3} - \frac{1}{16} \frac{f_t}{f_c} \frac{1 - \alpha - \overline{y}}{\overline{y}} \right) \right] + M_p, \tag{15}$$

where

$$M_p = \int_{a-l_p}^{a} q(w)(x_1 - x) b \, dx. \tag{16}$$

The bending moment M is equal to the moment on the cross-section due to the external loads and is given by $PS/4$ for the three-point bend beam (Fig. 1). Hence, the applied load P can be expressed by

$$P = \frac{4}{\beta} \left\{ bdf_t \left[\frac{A_f n}{bd} \frac{1}{\overline{y}} \left(\overline{y} + \alpha - \frac{d_0}{d} \right)^2 + \frac{\overline{y}^2}{3} + \frac{(1 - \alpha - \overline{y})^3}{\overline{y}} \times \left(\frac{1}{3} - \frac{1}{16} \frac{f_t}{f_c} \frac{1 - \alpha - \overline{y}}{\overline{y}} \right) \right] + \frac{M_p}{d} \right\}, \tag{17}$$

where $\beta = S/d$ is the span–depth ratio of the beam. From the solutions of Eq. (14) and Eq. (17), the loading capacity of the beam can be calculated once l_p and $q(w)$ are known.

4. Crack growth resistance curves (*R*-curves)

On the basis of mechanics of fracture a crack of length a will propagate when the stress intensity factor due to external loads, $K_P(a)$, balances the fracture resistance of the material, $K_R(a)$, i.e.,

$$K_P(a) = K_R(a). \tag{18}$$

The fracture resistance is the sum of the intrinsic fracture toughness of the plain concrete K_0, the contribution of the tensile FRP rods in the wake of the crack, $K_f(a)$, and the shielding effect due to the bridging stress within the FPZ, that is

$$K_R(a) = K_0 + K_f(a) + \int_{a-l_p}^{a} \frac{2q(x)}{\sqrt{\pi a}} F\left(\frac{x}{a}, \alpha\right) dx, \tag{19}$$

where $F((x/a), \alpha)$ is a geometrical dimensionless function that has been evaluated for a beam of infinite length [16] and may be given in the following form:

$$F\left(\frac{x}{a},\alpha\right)=\frac{3.52\left(1-\frac{x}{a}\right)}{(1-\alpha)^{3/2}}-\frac{4.35-5.28\frac{x}{a}}{(1-\alpha)^{1/2}}+\left[1-\alpha\left(1-\frac{x}{a}\right)\right]\times\left[0.83-1.76\frac{x}{a}+\frac{1.30-0.30\left(\frac{x}{a}\right)^{3/2}}{\sqrt{1-\left(\frac{x}{a}\right)^{2}}}\right]$$

and

$$K_{\mathrm{f}}=\frac{2T_{\mathrm{f}}}{\sqrt{\pi a}b}F\left(\frac{d_0}{a},\alpha\right). \tag{20}$$

From Eq. (19), it is clear that the R-curves of the beam can only be obtained when a described function of $q(x)$ is given. However, it is known that the bridging stresses in the FPZ satisfy Eq. (12), and a limit analysis of the R-curves can be easily performed. Inserting (9), (10) into (20) and replacing x_1 by $(\alpha+\overline{y})d$ in Eq. (20), the upper limit of the R-curves for a given value of l_{p} in Eq. (19) can be written as follows after considering Eq. (12)

$$K_R(a)=K_0+\frac{2f_{\mathrm{t}}}{\sqrt{\pi}}\sqrt{a}\left[\frac{A_{\mathrm{f}}n}{bd}\frac{1}{\alpha\overline{y}}\left(\overline{y}+\alpha-\frac{d_0}{d}\right)F\left(\frac{d_0}{a},\alpha\right)+\int_{\arcsin\frac{a-l_{\mathrm{p}}}{a}}^{\pi/2}F(\sin\gamma,\alpha)\cos\gamma\,\mathrm{d}\gamma\right]. \tag{21}$$

The lower limit of the R-curves can be obtained by omitting the integration in (21), i.e., by letting $l_{\mathrm{p}}=0$, which corresponds to the crack resistance of brittle fracture. Once the geometry of the FRP reinforced beam and the material properties of the plain concrete and the FRP rods, such as K_0, l_{p}, f_{t}, are given, the R-curves of the beam can be drawn from Eq. (21).

In engineering fracture, fracture toughness of a structure is defined as the fracture resistance at a particular crack length a_{c} at which the following condition is fulfilled:

$$\left.\frac{\partial K_P}{\partial a}\right|_{a=a_{\mathrm{c}}}=\left.\frac{\partial K_R}{\partial a}\right|_{a=a_{\mathrm{c}}} \tag{22}$$

To determine a_{c}, it is necessary to write the stress intensity factor of the cracked three-point bend beam due to the external load P

$$K_P(a)=\frac{3PS}{2bd^2}\sqrt{\pi a}H(\alpha), \tag{23}$$

where $H(\alpha)$ is also a geometric function which can be found from any handbook of stress intensity factors [16,17]. However, these factors are used for beams whose span-to-depth ratios are fixed to some specified values, e.g., 4 or 8. Thus the applications of these functions are limited. In the present paper, the following approximate expression, which is valid for any crack length and for any span-to-depth ratio larger than 2.5, is adopted [18]

$$H(\alpha)=\frac{1}{\sqrt{\pi}(1+3\alpha)(1-\alpha)^{3/2}}\left[p_0(\alpha)+\frac{4}{\beta}(p_1(\alpha)-p_0(\alpha))\right], \tag{24}$$

in which

$$p_0(\alpha)=1.99+0.83\alpha-0.31\alpha^2+0.14\alpha^3 \tag{25}$$

$$p_1(\alpha)=1.90+0.41\alpha+0.51\alpha^2-0.17\alpha^3 \tag{26}$$

Substituting (24) into (23), and then (18) and (22), solving the last two equations simultaneously, the critical crack length a_{c} can be determined numerically. If a_{c} is known the fracture toughness can be obtained using either Eq. (19) or (23).

5. Numerical results

In this section the new model is used to show the influence of a set of material and geometric parameters on the strengthening and R-resistance (toughening) of two lightly FRP-reinforced concrete three-point bend beams. The material properties of the plain concrete have been assumed [19]: $f_{\mathrm{c}}=23$ MPa, $E_{\mathrm{c}}=4730\sqrt{f_{\mathrm{c}}}$ MPa, $f_{\mathrm{t}}=0.62\sqrt{f_{\mathrm{c}}}$ MPa and $K_0=31$ MPa mm$^{1/2}$. The geometric parameters of the beams are shown in Table 1. The modulus of elasticity of the reinforcement FRP rods, E_{f}, is taken as 90 Gpa, if not stated otherwise.

In Figs. 5–8, the load capacity and the stress level in the FRP reinforcement are plotted against $(a-l_{\mathrm{p}})$ that represents a 'visible' crack depth, i.e., a practical measurable crack size in engineering applications.

Figs. 5 and 6 show the loading capacity (load–crack depth curves) predicted by the model for Case 1 and Case 2, respectively. The curves shown in these figures are the results corresponding to different lengths of the FPZ, in which the solid lines are for $l_{\mathrm{p}}=0$, i.e., the lower bounds of the loading capacity, while the others represent the upper bounds of the capacity associated with the given l_{p}. It can be seen that Mode I crack propagation is arrested after its growth to a certain

Table 1
Geometry of the three-point bend beam

Beam	Span S (mm)	Depth d (mm)	FRP location d_1 (mm)	Width b (mm)	Total area of FRP rods A_{f} (mm^2)	Initial notch a_0 (mm)
Case 1	1400	380	355	102	50.3	38
Case 2	1400	380	370	102	78.5	38

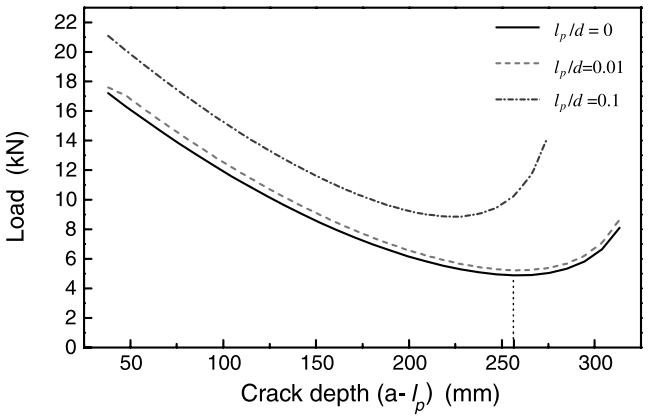

Fig. 5. Load capacity against crack depth for Case 1.

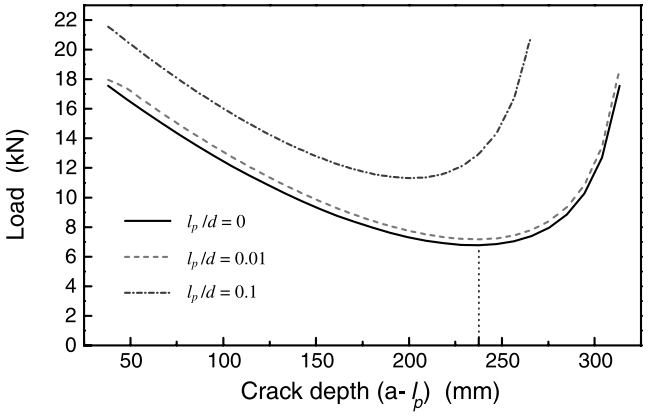

Fig. 6. Load capacity against crack depth for Case 2.

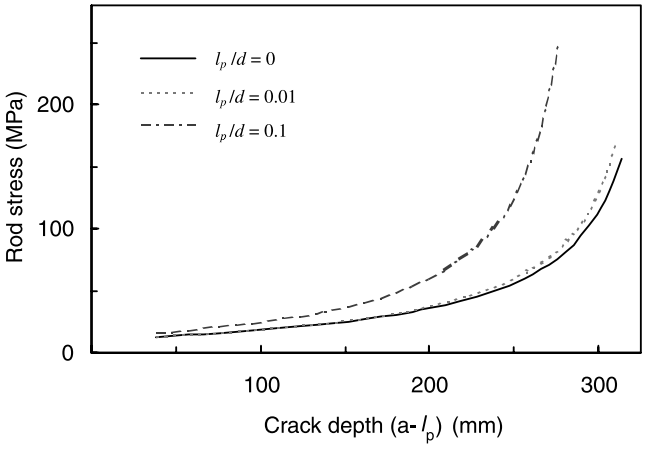

Fig. 7. Tensile stress in the reinforcement rod against crack depth (Case 1).

position depending on the length of the FPZ. A larger FPZ results in a smaller arrested crack and a higher load-bearing capacity. More over, compared with Case 1, Case 2 has a larger load capacity because the reinforcement ratio $(A_f/(b \times d))$ is higher and the FRP rods are closer to the bottom of the beam.

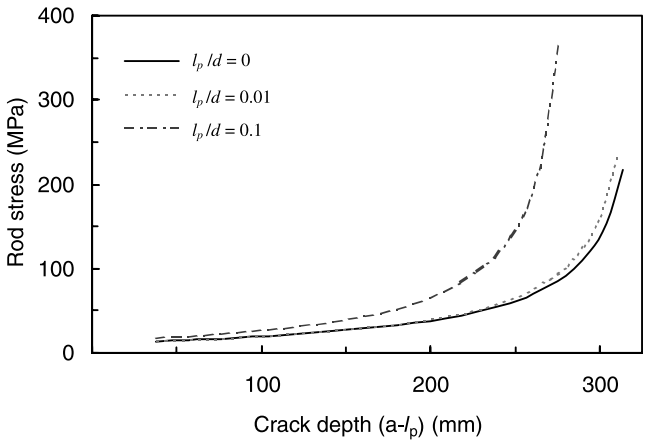

Fig. 8. Tensile stress in the reinforcement rod against crack depth (Case 2).

Figs. 7 and 8 show, respectively, the tensile stress levels in the reinforcement for both cases. Obviously, the tensile stress in the reinforcement increases with the propagation of the crack. For a fixed value of the crack depth, the stress is also increasing as the length of the FPZ increases, which, obviously, increases the total load carried by the beam.

Fig. 9 gives the loading capacity of a beam having the same properties as Case 1 except that the reinforcement area ($A_f = 100.6$ mm^2) is different. Compared with Fig. 5, it is observed that for the beam with higher reinforcement ratio, the crack depth at which the crack is arrested is shorter than the one corresponding to the beam with lower reinforcement. It is also observed that due to the high reinforcement ratio, the loading capacity corresponding to the arrested crack depth (Fig. 9) is greater than that of Case 1.

From Figs. 5, 6 and 9, it can be seen that there is a substantial drop in load capacity as the crack depth

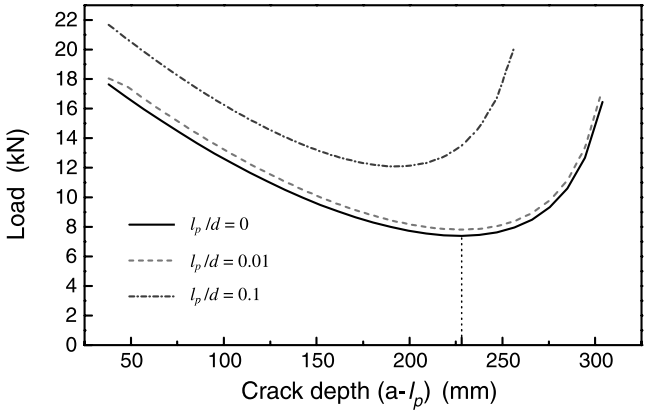

Fig. 9. Load capacity for Case 1 when $A_f = 100.6$ mm^2.

approaches a value at which stabilization occurs. In order to study this phenomenon, Figs. 10 and 11 are presented to show the effects of various parameters, such as reinforcement ratio, elastic stiffness of the reinforcement and length of the FPZ, upon the load capacity. Fig. 10 shows how the load capacity is influenced by the cross-sectional area of the reinforcement rod, i.e., the reinforcement ratio. In the figure, the solid curve is in fact identical to the dashed one in Fig. 5, which are for $A_f = 50.3$ mm^2 and $l_p/d = 0.01$. At the same value of l_p/d, when A_f is increased to 201.2 mm^2, four times greater than the initial reinforcement area (50.3 mm^2), the drop in load is still observed. However, the maximum relative drop in load is about 39% (dashed curve in Fig. 10), compared with a 70% drop in the lightly reinforced case (solid curve in Fig. 10). In the case of $A_f = 402.4$ mm^2, where the reinforcement ratio is almost doubled, the maximum relative drop in load is further reduced to about 20%. For a larger value of l_p/d, *e.g.*, $l_p/d = 0.1$, the relative drops in load are 58%, 28% and 11%, respectively, for the reinforcement areas of $A_f =$ 50.3, 201.2 and 402.4 mm^2. From these figures, it may be concluded that for a lightly reinforced beam a significant drop in load capacity is expected prior to stabilization.

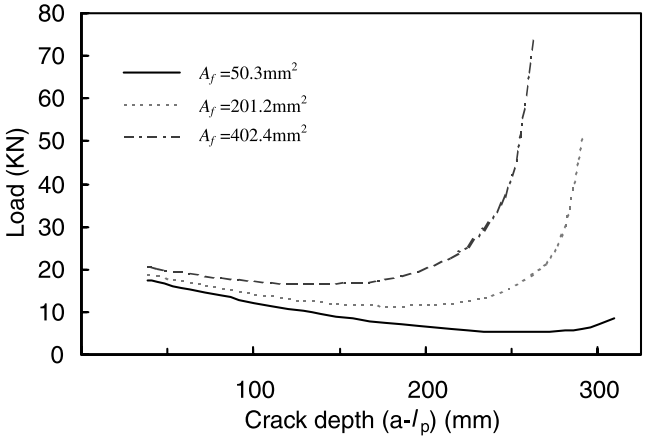

Fig. 10. Load capacity of the beam with different cross-sectional areas of the reinforcement rod when $l_p/d = 0.01$ (Case 1).

Similar observation can also be made when the elastic stiffness of the reinforcement rod varies. Fig. 11 gives the variation of the load capacity versus crack depth for various Young's moduli of the reinforcement rods. The range of the modulus represents the material properties of almost all the glass fiber and carbon fiber reinforced rods. It is evident that a beam with a higher stiffness reinforcement has a higher load capacity and a lower relative drop in load as the crack propagates.

Figs. 12 and 13 are, respectively, the fracture resistance curves for Case 1 and Case 2 for various sizes of FPZ. In general, the resistance increases with the increase of the size of the FPZ and the crack depth. At the initial stage of crack propagation, i.e., at small a/d, the increase of fracture resistance is very slow. After the crack depth reaches about $a/d = 0.6$ in both cases, the resistance increases rapidly. This means that more external load is required to maintain crack propagation. Similar crack resistance curves can also be seen in metal and ceramic matrix composites with bridging effects [20]. This is because the R-curve of a finite beam represents the apparent fracture resistance that always approaches infinity when the crack length approaches the depth of the beam. Fig. 14 shows the fracture toughness of the beams as the length of the FPZ varies. It is seen that the FPZ has a considerable effect on the fracture toughness of the beams. From the comparisons of Figs. 12–14, it is concluded that Case 2 provides more effective resistance to crack growth than that of Case 1.

The observations made on the curves shown in Fig. 5 to Fig. 14 demonstrate that an increase of the reinforcement ratio, the length of the FPZ and the stiffness

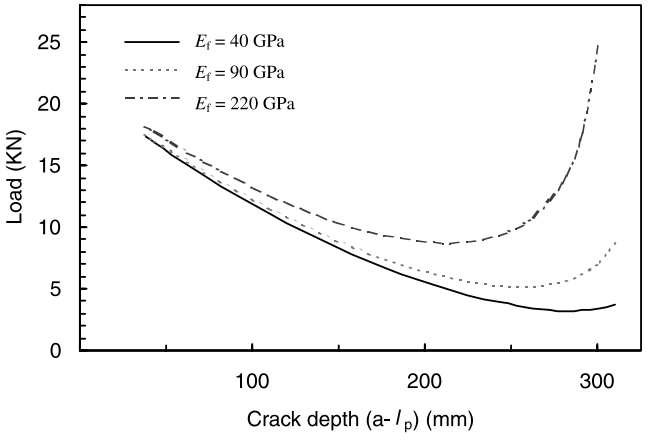

Fig. 11. Load capacity of the beam reinforced with FRP rods having various Young's moduli when $l_p/d = 0.01$ (Case 1).

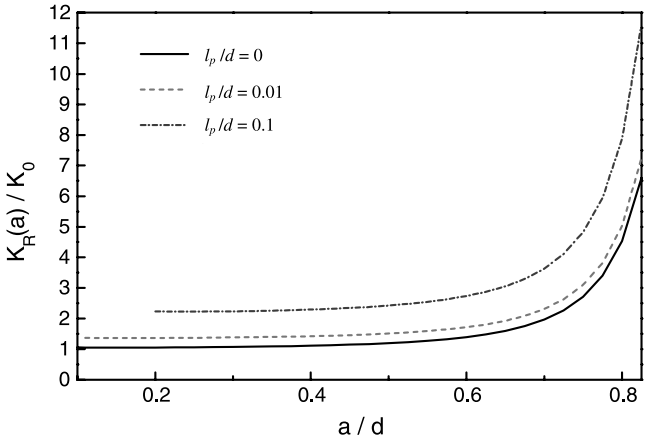

Fig. 12. Influence of the length of FPZ on resistance curves for Case 1.

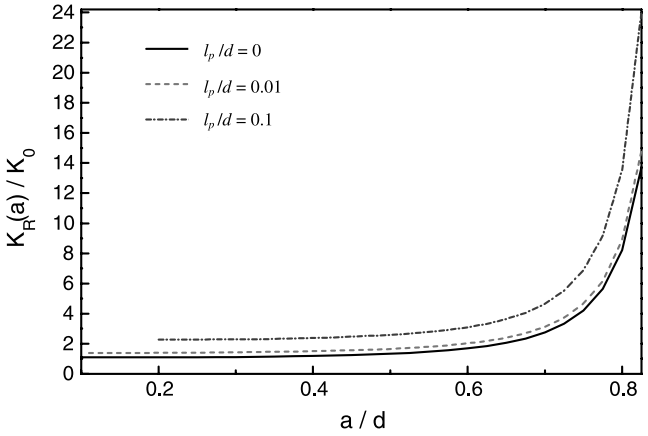

Fig. 13. Influence of the length of FPZ on resistance curves for Case 2.

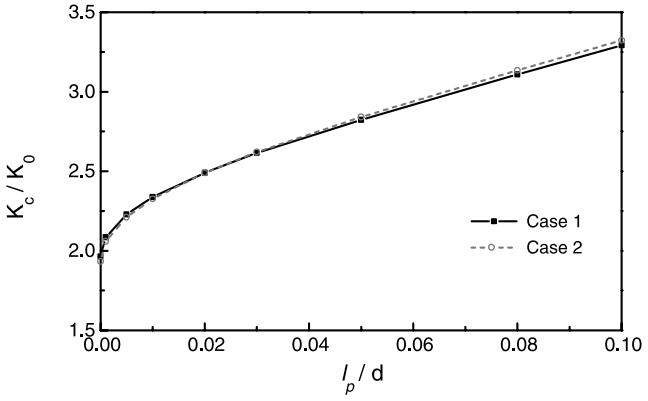

Fig. 14. Influence of the length of FPZ on fracture toughness.

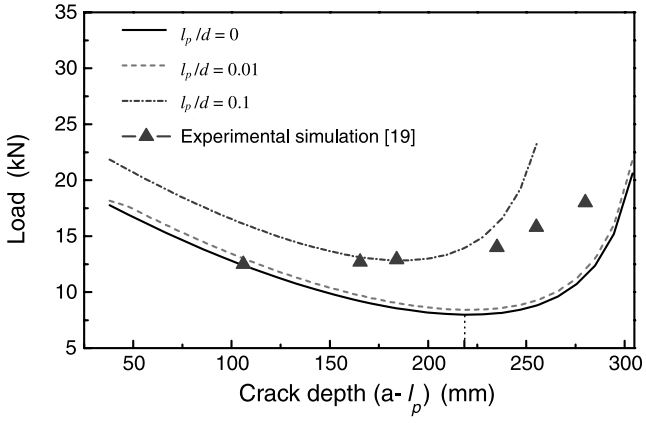

Fig. 15. Load capacity of beams with steel reinforcement (Case1).

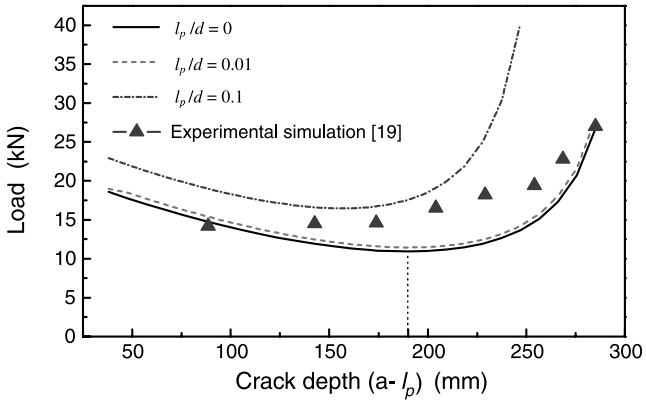

Fig. 16. Loading capacity of beams with steel reinforcement (Case2).

of reinforcement will increase the load capacity. They also demonstrate that geometric parameters, e.g., the initial crack length and the position of the reinforcement rods, also have significant influences on the structural behaviour of the beam.

To evaluate the model presented in this study, Figs. 15 and 16 show the comparisons of loading capacity (load–crack depth curves) between experimental results [19] and those predicted by the model. The experimental results were obtained from steel reinforced concrete beams for which the geometry and reinforcement ratio are the same as those of the FRP reinforced ones. The only difference is that the Young's modulus for steel is much higher than that of the FRP rods and is 209 (GPa). To make comparisons with the existing results, numerical results are obtained on the basis of present model by assuming that the reinforcement has an elasticity modulus of 209 GPa. Under this assumption, the calculated results are presented in Figs. 15 and 16 for, respectively, Case 1 and Case 2. It can be seen from the figures that the experimental results are bounded by the numerical results for $l_p = 0$ and $l_p/d = 0.1$. The comparisons shown in Figs. 15 and 16 suggest that l_p is small at the beginning of crack propagation, reaches its peak value after the crack grows to a certain length and then decreases as the crack propagates further. The FPZ becomes very small again when the crack propagates to the failure length of the beam, at which the crack ceases to propagate even when the external load is still increasing.

6. Conclusions

A theoretical method to predict loading capacity and fracture resistance of FRP reinforced concrete flexural beams has been developed. The constitutive law of FRP rods and the responses of plain concrete with appropriate tensile and compressive stresses were incorporated in the proposed model. The influence of the bridging stresses provided by the FPZ at the tip of fictitious fracture was examined.

It has been shown that the FPZ has a considerable effect on the arrest of the crack. Large FPZ is more

effective to increase both strengthening and resistance behaviour of the beams. Moreover, it has been observed that as a crack propagates, there is always a drop in the load capacity of the beam prior to stabilization. However, it has been concluded that in general, the drop in load decreases as the reinforcement ratio increases. Evidently, experimental investigations are needed, in this aspect, to verify the theoretical model. As a special case, the comparisons between the numerical results obtained and the existing experimental ones for an equivalent steel reinforced beam have shown that the present method can provide reliable results for the analysis of such structures.

It is also useful to notice that the size of the FPZ during crack propagation is not a constant.

Acknowledgements

The authors would like to acknowledge the support of EPSRC (grant no. GR/L91450). The authors are also grateful to the two anonymous referees for their helpful comments on an earlier version of this paper.

References

[1] Ghali A, Favre R. Concrete structures: stresses and deformations. London: E & FN Spon; 1994.
[2] ACI 440R-96, state-of-the-art report on fiber reinforced plastic reinforcement for concrete structures. Farmington Hills: American Concrete Institute; 1996.
[3] Bank LC, Puterman M, Katz A. The effect of material degradation on bond properties of fiber reinforced plastic reinforcing bars in concrete. ACI Mater J 1998;95(3):232–43.
[4] Clarke JL, editor. Structural design of polymer composites—EUROCOMP design code and handbook. UK: St Edmundsbury Press; 1996.
[5] Shah SP, Swartz SE, Ouyang C, editors. Fracture mechanics of concrete: applications of fracture mechanics to concrete, rock and other quasi-brittle materials. New York: John Wiley & Sons, Inc.; 1995.
[6] Hillberborg A, Modéer M, Petersson PE. Analysis of crack formation and crack growth in concrete by means of fracture mechanics and finite elements. Cement Concrete Res 1976;6(6):773–82.
[7] Ingraffea AR, Gerstle WH, Gergele P, Saouma V. Fracture mechanics of bond in reinforced concrete. J Struct Div, ASCE 1984;110(4):871–90.
[8] Karihaloo BL. Tension softening diagrams and longitudinally reinforced beams. In: Baker G, Karihaloo BL, editors. Fracture of brittle disordered materials: concrete, rock and ceramics. London: E & FN Spon Pub; 1995. p. 35–50.
[9] Foote RML, Mai YW, Cotterell B. Crack growth resistance curves in strain-softening materials. J Mech Phys Solids 1986;34(6):593–607.
[10] Gerstle WH, Dey PP, Prasad NNV, Rahulkumar P, Xie M. Crack growth in flexural members—a fracture mechanics approach. ACI Struct J 1992;89(6):617–25.
[11] Hilsdorf HK, Brameshuber W. Code-type formation of fracture mechanics concepts for concrete. Int J Fract 1991;51:61–72.
[12] Liaw BM, Jeang FL, Du JJ, Hawkins NM, Kobayashi AS. Improved non-linear model for concrete fracture. J Eng Mech, ASCE 1990;116(2):429–45.
[13] Cedolin L, Deipoli S, Iori I. Tensile behavior of concrete. J Eng Mech, ASCE 1987;113(3):431–49.
[14] Du J, Yon JH, Hawkins NM, Arakawa K, Kobayashi AS. Fracture process zone for concrete for dynamic loading. ACI Mater J 1992;89(3):252–8.
[15] Alvarado AM, Torrent RJ. The effect of the shape of the strain-softening diagram on the bearing capacity of concrete beam. Mater Struct 1987;20:448–57.
[16] Tada H, Paris P, Irwin G. The stress analysis of cracks handbook. Del Research Corporation, 1985.
[17] Murakami Y. Stress intensity factors handbook. New York: Pergamon; 1986.
[18] Guinea GV, Pastor JY, Planas J, Elices M. Stress intensity factor, compliance and CMOD for a general three-point-bend beam. Int J Fract 1998;89:103–16.
[19] Baluch MH, Azad AK, Ashmawi W. Fracture mechanics application to reinforced concrete members in flexure. In: Carpinteri A, editor. Applications of fracture mechanics to reinforced concrete (Chapter 16). London: Elsevier Applied Science; 1992. p. 413–36.
[20] Zok F, Hom CL. Large scale bridging in brittle matrix composites. Acta Metall Mater 1990;38(10):1895–904.